IMECE2012-86927

FUNCTIONALLY HETEROGENEOUS POROUS SCAFFOLD DESIGN FOR TISSUE ENGINEERING

AKM B. Khoda
Department of Industrial Engineering
University at Buffalo
Buffalo, NY   14260, USA

Bahattin Koc
Faculty of Engineering and Natural Sciences Sabanci
University, Istanbul 34956, Turkey
bkoc@buffalo.edu

ABSTRACT

Most of the current tissue scaffolds are mainly designed with homogeneous porosity which does not represent the spatial heterogeneity found in actual tissues. Therefore engineering a realistic tissue scaffolds with properly graded properties to facilitate the mimicry of the complex elegance of native tissues are critical for the successful tissue regeneration. In this work, novel bio-mimetic heterogeneous porous scaffolds have been modeled. First, the geometry of the scaffold is extracted along with its internal regional heterogeneity. Then the model has been discretized with planner slices suitable for layer based fabrication. An optimum filament deposition angle has been determined for each slice based on the contour geometry and the internal heterogeneity. The internal region has been discritized considering the homogeneity factor along the deposition direction. Finally, an area weight based approach has been used to generate the spatial porosity function that determines the filament deposition location for desired bio-mimetic porosity. The proposed methodology has been implemented and illustrative examples are provided. The effective porosity has been compared between the proposed design and the conventional homogeneous scaffolds. The result shows a significant error reduction towards achieving the bio-mimetic porosity in the scaffold design and provides better control over the desired porosity level. Moreover, sample designed structures have also been fabricated with a NC motion controlled micro-nozzle biomaterial deposition system.

Keyword: Deposition angle, Porosity function, variational filament distance.

1.   INTRODUCTION

In tissue engineering, porous scaffold structures are mainly used as supporting and guiding substrate towards the 3D tissue regeneration processes. The fundamental expectation from a functional scaffold is that it induces an amenable bio-reactor while stimulating the tissue regeneration processes with minimally upsetting the delicate equilibrium of the cellular microenvironment. Even though biocompatibility is crucial, but the structure itself must facilitate functions such as cell migration, proliferation, differentiation and wastes removal [1].

In bone tissue engineering, researchers [2] have invested in achieving a bio-mimetic scaffold design by mimicking the bone morphology. Such effort may represent the spatial material distribution for both cortical and cancellous bone segment but may not capture the regional heterogeneity in bone's spatial extrinsic and intrinsic properties [3]. Lal et al. [4] has proposed microsphere-packed scaffold modeling technique where the porosity is stochastically distributed throughout the structure. The achievable porosity range can be controlled with the size and number of microspheres and their packing conditions. In their other work [5], a heuristic based porous structure modeling has been developed using the constructive solid geometry (CSG) based approach and combining the Boolean function in a stochastic manner. Porous object with nested cellular structure has been proposed in literature [6, 7] which may introduce the gradient porosity along the architecture with the function based [8] geometry and topology variation in the unit-cell library. A three dimensional porous structure modeling technique has been proposed with layer based 2D Voronoi tessellation [9] which ensures the interconnected pore networks. In another work [10], geometric modeling of functionally graded material (FGM) has been proposed with graded microstructures. The gradient porosity in the FGM has been achieved with stochastically distributed voronoi cells. And the pore's shapes are tailored with B-Spline representation. Holdstein et al. [11] proposed a reverse engineering technique to generate the porous bone structure model with volumetric texture synthesis method. The method captures the stochastic and porous nature of the bone micro-structure into the reconstructed scaffold model. A hierarchical two level bone modeling technique [12] has been proposed considering the apparent density distribution and the surface-to-

volume ration distribution. The proposed model generates 3D bone structure with spatially distributed micro-structure that matches the stiffness of human bone under load condition. Current approaches for modeling of variational porosity in the scaffolds are mostly random and generate uncontrollable porosity. Limited control in spatial porosity may be achievable for some methods; however this may limit the true 3D porous characteristics as the interconnectivity and continuity among pores become uncertain. Hence deterministic mathematical methods to generate the representations of actual gradient in porosity and the pore geometry can provide better control to achieve the desired porous structure. In this work, a novel layer based heterogeneous porous structure modeling has been proposed to achieve the gradient porosity design.

The rest of the paper is organized as follows. Section 2 contains the novel variational porous scaffold structure modeling with controllable and variational porosity design. In sub-section 2.1, we discussed the geometric model extraction for the defected bone segment. Sub-section 2.2 describes the slice generation methodology along with the internal feature suitable for SFF technique. Section 2.3 and 2.4 describes the contour discretization and determine the optimum deposition angle considering the heterogeneity of the scaffolding area. Section 2.5 determines the spatial function for optimum filament location to achieve desired porosity. The proposed design has been implemented in Section 3 and bio-fabrication has been shown in Section 4. And finally, we draw conclusions in Section 5.

2. METHODOLOGY

2.1 3D Heterogeneous Model Extraction

The regional heterogeneity exists in bone, which allows bone to perform its multi-objective functionality i.e. mechanical, biological and chemical functions simultaneously. Such regional heterogeneity in bone could be consolidated into combination of internal homogeneous features to discritize the bone model in 3D space. The geometric significance (i.e. location, size, shape) of such internal extrinsic features or the heterogeneity for the defected bone segment can be obtained by analyzing the MRI or CT image for bone mineral density, bone texture analysis via micro-beam X-ray radiation, feature recognition algorithms [13]. Besides, spatial/heterogeneous porosity in bone structure has been reported in literature [14, 15] with clear contrast of regional porosity by analyzing the real human bone structure. Fig. 1(a) shows the porosity distribution in the proximal femur [14]. Moreover, spatial density and surface-to-volume ration distribution in 3D bone has been modeled in [12]. These spatially distributed 3D features might represent uniform properties individually and their combination could capture the anisotropy in bone structure. The accuracy of such representation for bone anisotropy might be a subject of proper data evaluation algorithm or methodology and beyond the scope of this paper. The reconstructed model should have a set of iso-property regions to represent the heterogeneous property of bone which

may not be axisymmetric or uniform in shape as show in Fig. 1(b,c). The corresponding property for each iso-region can also be interpreted as uniform property or iso-porosity regions and thus the term iso-porosity and iso-property have been used alternatively in this paper. Moreover, any segment or layer containing more than one iso-property region is referred as heterogeneous region in this paper.
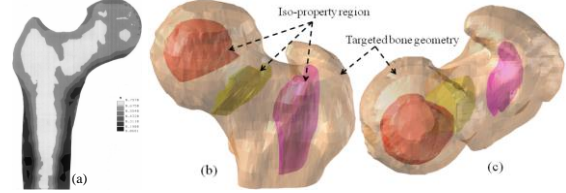

Fig. 1. (a) Average porosity distribution in the proximal femur (midcoronal plane) [14] (b) Perspective view (c) top view of targeted bone geometry with internal iso-property regions that represent the regional heterogeneity.

2.2 Slice Generation

The generated surfaces along with the internal features are sliced for layered manufacturing by a set of parallel intersecting planes. By connecting the intersection points between the plane and the surfaces would generate non-self intersecting, closed, planar contours. The distance between the intersecting planes can be constant in uniform slicing which is usually the diameter of deposited filament by the SFF system. Thus a set of parallel slicing contours represent the targeted bone geometry $S = \{s_k\}$ where k is the number of contour slice for the bone segment. The kth contour of the bone geometry and the corresponding internal iso-porosity contours have been shown in the following figure (Fig. 2) as an example.
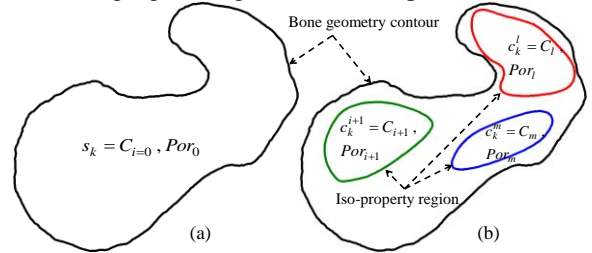

Fig. 2. A sample slice of bone (a) only outer contour and (b) the corresponding internal iso-porosity contours.

The outer contour s_k contains all the iso-porosity contour curves inside it, $C_k = \{c_k^1 .. c_k^m\}$ where m is the number of iso-porosity contour in k^{th} slice. Thus each layer is defined by a set of iso-porosity contour curves embedded in the outer slice contour i.e. $C = \{C_0 = s_k, C_k\} = \{C_i\}_{i=0,..m}$. Each contour C_i is assigned with a desired porosity defined by Por_i which represent the porosity of ith contour. All contour curves are simple planner closed curve i.e. the planner curve does not intersect itself other than its start and end points and have the same (positive) orientation. And the general equation for these contours can be parametrically represented as-

$$C_i(u_i) = (x(u_i), y(u_i)) \qquad \forall i = 0,..m$$
$$u_i \in [a_i, b_i] \qquad\qquad (1)$$
$$C_i(a_i) = C_i(b_i)$$

Here, $C_i(u_i)$ represent the parametric equation for i^{th} contour with respect to parameter u_i at a range between $[a_i, b_i]$.

2.3 Contour discretization and weight determination

The targeted regions first need to be discretized based on the heterogeneity factor. A set of parallel lines can be used for discretization and the area generated between two adjacent parallel lines can be analyzed for heterogeneity. These intersecting parallel lines might be equidistant from each other i.e $h_t = h_s$ or varying distant $h_t \neq h_s$ where both h_t and h_s are variables. Thus the combination of such design parameters can virtually be infinite which could be computationally extensive. To avoid such computational complexity, a novel rectilinear bounding box technique has been introduced [13] that would eventually reduce the feasible solution region significantly without compromising the optimality.
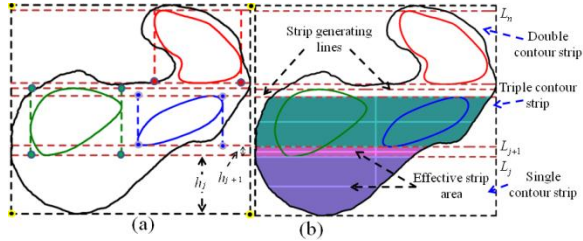

Fig. 3. (a) Generating the strips with rectilinear bounding box approach (b) effective strip area and their heterogeneity.

After discritizing the region with strips, the area based heterogenity weight [13] for each strips has been calculated by using the following Equation (2).

$$Weight\_ST_j = \left(\left(A_j - \sum_{i=1}^{m} CA_{A_j}^i\right) + \sum_{i=1}^{m}\left(CA_{A_j}^i \times het_j^{Contour}\right)\right) \times het_j^{Property} \ \forall j$$
$$(2)$$

Where, $Weight\_ST_j$ is the weight; A_j is the effective area, $CA_{A_j}^i$ is the area of ith contour contributed to the effective area; $het_j^{Contour}$ and $het_j^{Property}$ are the heterogeneity factor due to contour and property of jth strip. And the total weight of the slice can be calculated by adding individual strip's weight.

$$Total\_Weight = \sum_{j=1}^{n} Weight\_ST_j \qquad (3)$$

Here, $Total\_Weight$ is the accumulated total weight. This accumulated weight is a non-linear function of contributed area and in ideal case i.e. for complete homogeneous region, the weight would be minimum. Increasing the heterogeneity would increase the weight of the slice.

2.4 Filament deposition direction

From the above section, it is clear that changing the strip orientations i.e. filament deposition direction would generates a new set of strip. And by using the same methodology described in previous Section 2.3, the weight can be determined. To identify the optimum deposition direction over the heterogeneous region, a reference frame concept has been developed [13]. The weight at every θ interval of the frame angle $\theta \in [0, \pi]$ needs to be determined and the optimum deposition direction would be the corresponding minimum weight value.

$$\text{Min } \{Total\_Weight_k^\theta\}$$
$$\text{Subject to -}$$
$$\sum_{j=1}^{n} A_j = \Omega_k$$
$$(4)$$
$$\sum_{i=1}^{m} (CA_{A_j}^i \,|\, (n_{i,j} \geq t_{i,j} \geq 1; n_{i,j-1} \geq t_{i,j-1} \geq 1)) = A_j \quad \forall \ i, j$$
$$\theta_k \in [0, \pi] : k = 0$$
$$\theta_k \in [\theta_{k-1}^* + \alpha, \ \theta_{k-1}^* + \beta] : k > 0$$

Here, $\{Total\_Weight_k^\theta\}$ represent a set of the total weight for every θ interval in k^{th} slice where the individual element of this set can be calculated with Equation (3). Ω_k is the total area of kth slice. The optimum deposition direction or frame angle θ_k^* for k^{th} slice can be calculated from Equation (4). The angle α and β are the acceptable angle range between consecutive layers to ensure the structural integrity and continuity. The segment of deposited material, that passes through the heterogeneous region may not be eliminated completely with the optimum deposition angle θ_k^*, but this deposition direction may reduce the overall heterogeneity effect significantly.

2.5 Location Function for filament deposition

After getting the optimum filament deposition directions θ_k^* with corresponding strip set $ST^{\theta_k^*} = \{st_j^{\theta_k^*}\}_{j=1,..n}$, and their generating line set $L^{\theta_k^*} = \{L_j^{\theta_k^*}\}_{j=0,..n}$; a function based filament distance determination methodology has been implemented to determine the optimum filament location individually. The proposed function needs to be implemented for all strips $ST^{\theta_k^*}$ at the optimum filament deposition directions θ_k^* as shown in Fig. 4.
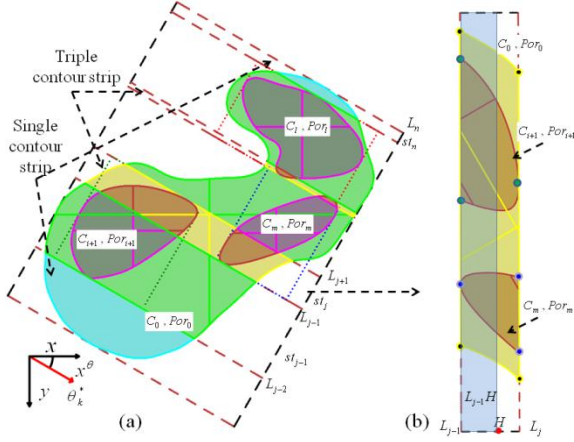
Fig. 4. (a) Function generation for the slice with the optimum deposition angle θ_k^* (b) a heterogeneous triple contour j^{th} strip st_j

The functional area for each contributing contours along the width of the strip have been plotted as shown in Fig. 5. The porosity function, FP for any segment ΔH in the strip can be calculated by the following equation where, $\Delta H \to 0$ and is the function of strip width and its contour property.

$$FP_j(\Delta H) = \sum_{i=0}^{m} \frac{FA_j^i(\Delta H)}{A_j(\Delta H)} \times Por_i \quad \forall\ j, FA_j^i > 0; \quad (5)$$

Where, $FP_j(\Delta H)$ is the porosity function for j^{th} strip with a finite segment ΔH shown in Fig.5 and is calculated by considering the percentage weighted area contribution and their corresponding porosity.
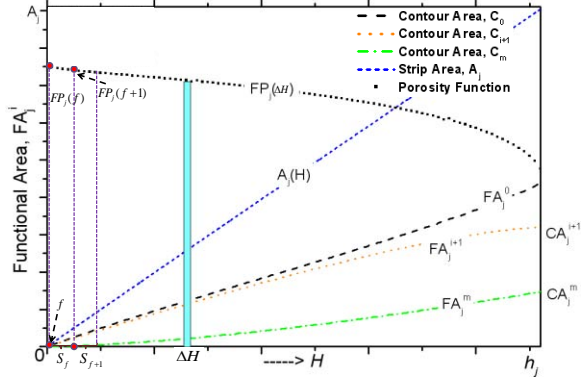

Fig. 5. Filament positional function determination for j^{th} strip st_j, a heterogeneous triple contour.

For evaluation purpose the porosity deviation from the designed one to the desired porosity has been calculated by Equation 6.

$$E = \sum_{j=0}^{n} \sum_{i=0}^{m} \left(\left| FP_j(f) - Por_i \right| \right) \times FA_j^i(f) \quad \forall\ f \quad (6)$$

Where, E is the resultant porosity evaluation index.

3. IMPLEMENTATION

The proposed techniques have been implemented on 2.3 GHz PCs using Rhino Script and Visual Basic programming languages in a femur slice with three internal iso-porosity regions and their designed property has been presented in Table 1.

Table 1 Contour property for femur slice.

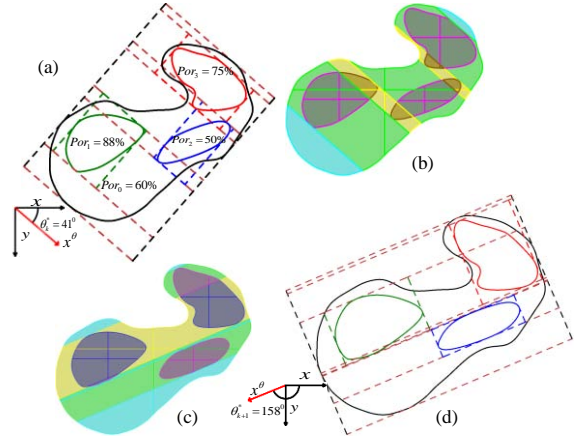| Contour, C_i	Porosity, Por_i	Area, mm²
C_0	$Por_0 = 60\%$	199.95
C_1	$Por_1 = 88\%$	50.81
C_2	$Por_2 = 50\%$	27.85
C_3	$Por_3 = 75\%$	48.79

Fig. 6. Consecutive heterogeneous femur slices with three iso-porosity region; optimum filament deposition angle (a-b) $\theta_k^* = 41^0$ and (c-d) $\theta_{k+1}^* = 158^0$ and associated strips respectively.

To get the optimum deposition angle, the internal region has been discretized with strips generated from the bounding box method described in Section 2.3. The optimum deposition direction or frame angle for two consecutive slices k^{th} and $(k+1)^{th}$ have been achieved as $\theta_k^* = 41^0$ and $\theta_{k+1}^* = 158^0$ respectively as shown in Fig. 6. Spatial porosity function for both layer have been determined and plotted in the following figure (Fig. 7). The lower horizontal axis represents the strip width for the 1st layer ($\theta_k^* = 41^0$) and the upper horizontal axis represents the consecutive second layer $\theta_{k+1}^* = 158^0$.
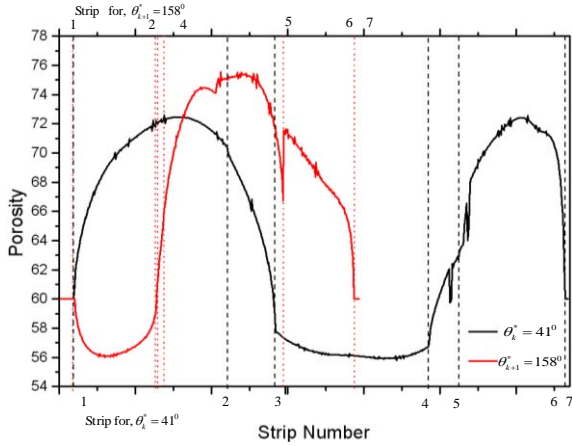
Fig. 7. Porosity function for consecutive optimum layer of femur slice.

The porosity function clearly represents the heterogeneity within the strip, as higher heterogeneity introduce higher deviation in the porosity range to minimize the disparity. The sample has been designed with 100 micrometer filament diameter to determine the filaments location following the porosity function. Moreover a bi-layer membrane has been shown and the porosity has been evaluated for the generated anisotropic pore-cells as shown in the Fig. 8.
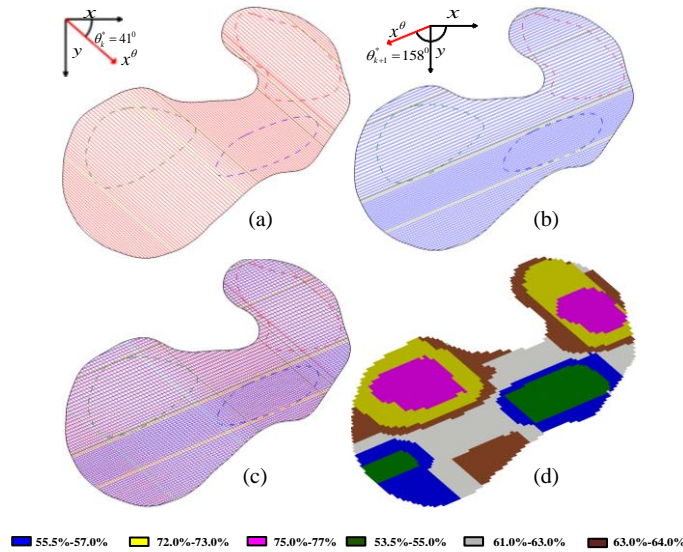

Fig. 8. Variational filament locations following the porosity function (a) for the 1st layer (b) consecutive 2nd layer (c) combined layer (d) porosity gradient for the combined layer (designed with 100 micrometer filament diameter).

Even though each layer has been optimized for the filament location, but consecutive layers need to be combined to measure the spatial porosity within the regions. Because of the variational distance between filaments, the pore cell become highly anisotropic in nature and the porosity for the structure become true gradient which follow the heterogeneity of the internal regions as shown in Fig. 8. Also, the deviation data has been calculated and compared and plotted with a 68% constant porosity membrane in the Fig. 9 which is always lower than the traditional homogeneous structure.
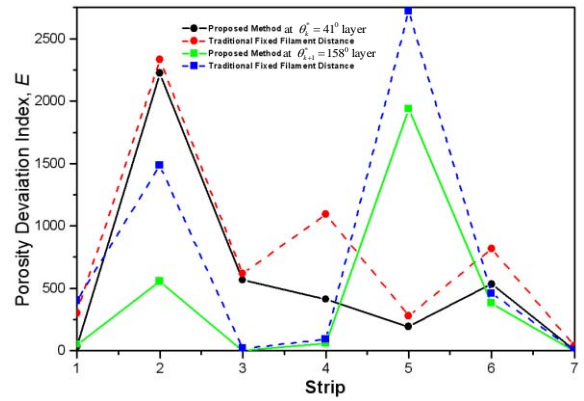

Fig. 9. Porosity deviation index for both layer compared with proposed method and average 68% porosity.

4. BIO-FABRICATION

For demonstration purpose, two consecutive slices of the above examples have been considered for fabrication with a NC motion controlled micro-nozzle biomaterial deposition system [16]. To fit into the working envelope of the fabrication system, the actual human femur model has been scaled down by 70%. The corresponding area and the iso-porosity remain the same as presented in Table 1. The filament location has been generated using the methodology described in Section 2 with 200 μm substrate diameter. The fabrication model has been shown in Fig. 10(b). A total 50 and 31 number of filament has been generated for the kth and $(k+1)^{th}$ slice respectively where the location for each of these layers have been determined from the porosity function. During the tool-path generation, full connectivity may not be possible due to the concavity in the outer region which is common in free-form shape. To ensure the connectivity, motion without deposition may need to be introduced as shown in Fig. 10(a).
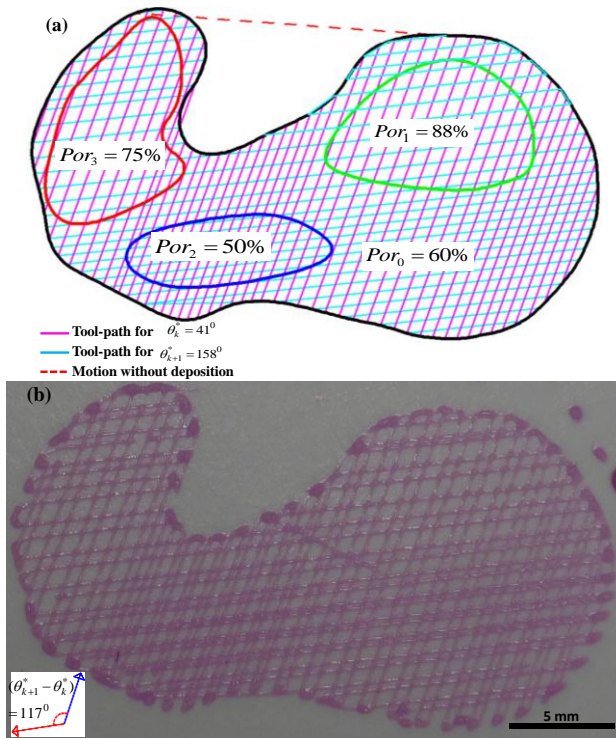
Figure 10. (a) Heterogeneous femur slice with three defined iso-porosity regions (b) and its sample fabrication with 200 micro meter filament diameter.

The fabricated model has been characterized by using IMAGEJ software. To avoid measuring complexity, no partial pore cells are considered during the image analysis. For unbiased sampling during the average porosity calculation, we tried to measure 1 pore cells in every $2mm^2$ area of the fabricated sample. As shown in the table, the porosity varies within the iso porosity regions but the average porosity matches the desired porosity pattern. The calculated porosity in some iso-porosity regions shows a wide range of porosity than expected. This is because of the deposition system accuracy level. Moreover, for some contours the measured average error is significantly higher but the overall percentage area for those contours are smaller. The methodology incorporates an adjustment technique between the error level and the corresponding weight so that the overall error of the structure remains reasonable ($\approx$ 4%) as shown in Table 2.

Table 2. Porosity characterization of the fabricated model.

Average filament diameter, μm	Average angle between layers, Deg	Avg. calculated porosity (%), in region				Porosity range(%), in region				Avg. Error (%), in region				Area Weighted error (%)
		C_0	C_1	C_2	C_3	C_0	C_1	C_2	C_3	C_0	C_1	C_2	C_3	
197	116.8	62	82	54	78	54-78	76-84	49-64	74-84	3.3	-6.8	8	4	4.35

5. CONCLUSION

In this research, a novel layer based heterogeneous scaffold modeling has been developed with functionally gradient porosity. The design methodology generates spatial variational porosity following the heterogeneity of the internal regions. An optimum filament deposition angle for layers has been determined by considering spatial in-homogeneity. A function based approach has been proposed to determine the actual filament location that can minimize the heterogeneity effect while attaining the desired (bio-mimetic) porosity as close as possible. The proposed method minimizes the deviation between the desired and design property as well as follow the spatial heterogeneity by generating a controllable, continuous and fabricatable structure design. Moreover the proposed technique provides better control on the achievable porosity in the heterogeneous space ensuring structural continuity and fabricatability. The proposed methodology has been implemented on a bi-layer structure; but stacking the bi-layer designed structure consecutively can generate the 3D scaffold with the desired porosity distribution.

REFERENCES

[1] Khoda, A., and Koc, B., 2012, "Designing Controllable Porosity for Multi-Functional Deformable Tissue Scaffolds," ASME Transactions, Journal of Medical Device (In Press).

[2] Geffre, C. P., Margolis, D. S., Ruth, J. T., DeYoung, D. W., Tellis, B. C., and Szivek, J. A., 2009, "A novel biomimetic polymer scaffold design enhances bone ingrowth," Journal of Biomedical Materials Research Part A, 91A(3), pp. 795-805.

[3] Zioupos, P., Cook, R. B., and Hutchinson, J. R., 2008, "Some basic relationships between density values in cancellous and cortical bone," Journal of Biomechanics, 41(9), pp. 1961-1968.

[4] Lal, P., and Sun, W., 2004, "Computer modeling approach for microsphere-packed bone scaffold," Computer-Aided Design, 36(5), pp. 487-497.

[5] Schroeder, C., Regli, W. C., Shokoufandeh, A., and Sun, W., 2005, "Computer-aided design of porous artifacts," Computer-Aided Design, 37(3), pp. 339-353.

[6] Fryazinov, O., Vilbrandt, T., and Pasko, A., "Multi-scale space-variant FRep cellular structures," Computer-Aided Design(0).

[7] Wettergreen, M. A., Bucklen, B. S., Starly, B., Yuksel, E., Sun, W., and Liebschner, M. A. K., 2005, "Creation of a unit block library of architectures for use in assembled scaffold engineering," Computer-Aided Design, 37(11), pp. 1141-1149.

[8] Pasko, A., Fryazinov, O., Vilbrandt, T., Fayolle, P.-A., and Adzhiev, V., 2011, "Procedural function-based modelling of volumetric microstructures," Graphical Models, 73(5), pp. 165-181.

[9] Chow, H. N., Tan, S. T., and Sze, W. S., 2007, "Layered Modeling of Porous Structures with Voronoi Diagrams," Computer-Aided Design & Applications, 4(1-4), pp. 321-330.

[10] Kou, X. Y., and Tan, S. T., 2011, "Microstructural modelling of functionally graded materials using stochastic

Voronoi diagram and B-Spline representations," International Journal of Computer Integrated Manufacturing, 25(2), pp. 177-188.

[11] Holdstein, Y., Podshivalov, L., and Fischer, A., 2011, "Geometric modeling and analysis of bone micro–structures as a base for scaffold design Advances on Modeling in Tissue Engineering," P. R. Fernandes, and P. J. Bártolo, eds., Springer Netherlands, pp. 91-109.

[12] Coelho, P. G., Fernandes, P. R., Rodrigues, H. C., Cardoso, J. B., and Guedes, J. M., 2009, "Numerical modeling of bone tissue adaptation—A hierarchical approach for bone apparent density and trabecular structure," Journal of Biomechanics, 42(7), pp. 830-837.

[13] Khoda, A. B., and Koc, B., 2012, "Bio-mimetically Designed Functionally Gradient Porous Scaffold Structure for Tissue Engineering," CAD (Submitted).

[14] Pietruszczak, S., Inglis, D., and Pande, G. N., 1999, "A fabric-dependent fracture criterion for bone," Journal of Biomechanics, 32(10), pp. 1071-1079.

[15] Hosokawa, A., 2010, "Effect of porosity distribution in the propagation direction on ultrasound waves through cancellous bone," Ultrasonics, Ferroelectrics and Frequency Control, IEEE Transactions on, 57(6), pp. 1320-1328.

[16] Khoda, A., Ozbolat, I. T., and Koc, B., 2011, "A functionally gradient variational porosity architecture for hollowed scaffolds fabrication," Biofabrication, 3(3), pp. 1-15.